

Drastic facilitation of the onset of global chaos in a Hamiltonian system due to an extremum in eigenfrequency vs energy

S.M. Soskin¹, O.M. Yevtushenko^{2,3}, and R. Mannella⁴

¹*Institute of Semiconductor Physics, National Academy of Sciences of Ukraine, Kiev, Ukraine*

²*Institute of Radiophysics and Electronics, National Academy of Sciences of Ukraine, Kharkov, Ukraine*

³*Max-Planck-Institut für Physik komplexer Systeme, D-01187, Dresden, Germany*

⁴*Dipartimento di Fisica, Università di Pisa and INFN UdR Pisa, 56100 Pisa, Italy*

(February 9, 2020)

The Chirikov resonance-overlap criterion predicts that global chaos occurs only if at least two nonlinear resonances overlap in energy, which is conventionally assumed to require a non-small magnitude of perturbation. However, we show that the onset of global chaos in *zero-dispersion* systems, i.e. those whose eigenfrequency possesses an extremum as a function of energy, may occur at unusually *small* magnitudes of perturbation. It is possible due to the combination of the overlap in energy between different-order resonances and the overlap in the phase space between resonances of the same order. One of the most pronounced manifestations of this effect is a drastic increase of the energy range involved into the unbounded chaotic transport in spatially periodic system driven by a rather weak time-periodic force, provided the driving frequency approaches the extremal eigenfrequency or its harmonics.

05.45.Ac, 05.45.Pq, 75.70.cn

A perturbation of a Hamiltonian system typically causes the onset of chaotic layers in the phase space around separatrices of the unperturbed system and/or separatrices surrounding nonlinear resonances generated by the perturbation itself [1–3]: the system may be transported along the layer random-like. Chaotic transport plays an important role in many physical phenomena [3]. If the perturbation is weak then the layers are thin and such chaos is called *local* [1–3]. As the magnitude of the perturbation increases, the width of the layer grows and the layers corresponding to adjacent separatrices reconnect at certain (typically non-small) critical values of the magnitude, which marks the onset of *global* chaos [1–3].

In the *present* work, we demonstrate on an example of some periodically perturbed system that the reconnection of chaotic layers around different separatrices of the unperturbed system may be significantly facilitated by the layers associated with nonlinear resonances. Namely, there are certain frequencies in the close vicinity of which the critical values of the amplitude of perturbation are much smaller than those ones beyond these frequency ranges. This is closely related to the phenomenon of *zero-dispersion nonlinear resonance* [4–6] (cf. also studies of related maps [7–9]). The eigenfrequency ω as a function of energy E is equal to zero at the energies corresponding to the adjacent separatrices while possessing the local maximum $\omega_m \equiv \omega(E_m)$ between them. If the frequency of perturbation is close to ω_m and/or its multiples, the chaotic layers associated with nonlinear resonances reconnect with each other while each of them has reconnected the chaotic layer around the corresponding separatrix of the unperturbed system, thus providing for a chaotic transport in a broad energy range.

A drastic facilitation of the onset of global chaos in the systems with two or more separatrices is, in fact, just the

most pronounced manifestation of the more general phenomenon, namely the facilitation of the onset of global chaos in an arbitrary zero-dispersion system through the combination of the overlap in energy between resonances of different orders and the overlap in the phase space between resonances of the same order.

For more detailed consideration, we use as an example of a Hamiltonian system possessing more than one separatrix a potential system with a periodic potential possessing two different-height barriers in a period (Fig. 1(a)):

$$H_0(p, q) = \frac{p^2}{2} + U(q), \quad U(q) = \frac{(\Phi - \sin(q))^2}{2}, \quad (1)$$

$$\Phi = \text{const} < 1.$$

The model (1) may describe e.g. a 2D electron gas in the one-dimensional periodic magnetic field [10,11]. The interest to this system arose due to technological advances of the last decade allowing to manufacture high-quality magnetic superlattices (see e.g. [12,13]) leading to a variety of interesting behaviours of charge carriers in semiconductors (see e.g. [10–15] and references therein).

The separatrices of the Hamiltonian system (1) in the $p - q$ plane and the dependence of the frequency ω of its eigenoscillation on energy $E \equiv H_0(p, q)$ are shown in Figs. 1(b) and 1(c) respectively. As it is seen from the latter, $\omega(E)$ is close to the extreme eigenfrequency ω_m in the major part of the energy range between barriers levels $[E_b^{(1)}, E_b^{(2)}]$ while sharply decreasing to zero as E approaches $E_b^{(1)}$ or $E_b^{(2)}$. Such features of $\omega(E)$ are typical for most of systems with two or more separatrices.

Let the time-periodic perturbation be added [16]:

$$\dot{q} = \frac{\partial H}{\partial p}, \quad \dot{p} = -\frac{\partial H}{\partial q},$$

$$H(p, q) = H_0(p, q) - hq \cos(\omega_f t). \quad (2)$$

Let us first consider the evolution of chaos in the system (2)-(1) as h grows while ω_f remains fixed at some arbitrarily chosen value beyond the immediate vicinity of ω_m and its harmonics. It is well illustrated by Fig. 2. At small h , there are two thin chaotic layers, around the inner and outer separatrices of the undriven system. Note that unbounded chaotic transport takes place only in the outer chaotic layer i.e. in a *narrow* energy range. As h grows, so also do the layers until, at some critical value $h_{gc} \equiv h_{gc}(\omega_f)$, they merge. This event may be considered as the onset of global chaos: the whole range of energies between the barriers levels then becomes involved in unbounded chaotic transport. Note that the states $\{I^{(l)}\} \equiv \{p = 0, q = \pi/2 + 2\pi l\}$ and $\{O^{(l)}\} \equiv \{p = 0, q = -\pi/2 + 2\pi l\}$ (where $l = 0, \pm 1, \pm 2, \dots$) in the stroboscopic (for instants $n2\pi/\omega_f$ with $n = 0, 1, 2, \dots$) Poincaré section are associated respectively with the inner and outer saddles of the undriven system, and necessarily belong to the inner and outer chaotic layers respectively. Thus, the necessary and sufficient condition for global chaos to arise in our system may be formulated e.g. as the possibility for the system placed initially in the state $\{I^{(0)}\}$ to pass beyond the neighbouring “outer” states, $\{O^{(0)}\}$ and $\{O^{(1)}\}$, i.e. for $q(t \gg 2\pi/\omega_f)$ to become smaller than $-\pi/2$ or larger than $3\pi/2$.

A diagram in the $h - \omega_f$ plane, based on the above criterion, is shown in Fig. 3. The lower boundary of the shaded area represents the function $h_{gc}(\omega_f)$. It has deep cusp-like minima (*spikes*) at frequencies $\omega_f = \omega_s^{(n)}$ that are slightly less than the odd multiples of ω_m ,

$$\omega_s^{(n)} \approx \omega_m(2n - 1), \quad n = 1, 2, \dots \quad (3)$$

The deepest minimum occurs at $\omega_s^{(1)} \approx \omega_m$: $h_{gc}(\omega_s^{(1)})$ is approximately 40 times smaller than in the neighbouring pronounced local maximum of $h_{gc}(\omega_f)$ at $\omega_f \approx 1$. As n increases, the corresponding minimum becomes less deep. The origin of the spikes becomes obvious from the analysis of the evolution of the Poincaré section as h grows while $\omega_f \approx \omega_s^{(1)}$. For $h = 0.001$, one can see in Fig. 4(a) four chaotic trajectories: those associated with the inner and outer separatrices of the undriven system [1–3] are coloured green and blue respectively, while the trajectories associated with the nonlinear resonances of the 1st order [1–3] are indicated by red and cyan (the corresponding attractors are indicated respectively by crosses of the same colours). Examples of non-chaotic (often called KAM [1–3]) trajectories separating the chaotic ones are shown in brown. As h increases to $h = 0.003$ (Fig. 4(b)), the blue and red chaotic trajectories merge: the resulting trajectory is shown in blue. As h increases further (see Fig. 4(c), where $h = 0.00475$), the latter trajectory merges with the cyan chaotic trajectory (the resulting trajectory is shown by blue) and,

finally, as h increases slightly more (see Fig. 4(d), where $h = 0.0055$), the latter trajectory merges with the green trajectory [17], so that the inner well becomes involved in unbounded chaotic transport, thereby marking the onset of global chaos in our system, as defined above.

The chaotic character of motion on the trajectory associated with the separatrix of the undriven system can be considered [2] to be a consequence of the overlap of high-order resonances (in the case shown in Fig. 4(a), the relevant orders are 3, 5, 7, ...). The scenario described above for the onset of global chaos therefore corresponds exactly to the *combination* of an overlap between resonances of different orders (1, 3, 5, ...) and an overlap between resonances of the same (1st) order. Similarly, for the spikes of the higher order, the overlap between higher-order resonances is relevant.

The overlap between the resonances of the *same* order is called ZDNR/NR transition [5,6] and it may be quite well described [5,6] within the resonance approximation [1–3] as the separatrix reconnection [5–9]. Given that it plays the major role in the above scenario, the function $h_{gc}(\omega_f)$ near the spikes may also be quite well approximated using the resonance approximation. The explicit asymptotic (for $\Phi \rightarrow 0$) formulae for the minima themselves, in the lowest order of the parameters of smallness, are as follows:

$$\omega_s^{(n)} \approx (2n - 1)\omega_m \approx \frac{(2n - 1)\pi}{2 \ln(\frac{8}{\Phi})}, \quad n = 1, 2, \dots, \quad (4)$$

$$\Phi \ll 1,$$

$$h_{gc}(\omega_s^{(n)}) \approx \frac{(2n - 1)}{24} \Phi^3 \ln(\frac{8}{\Phi}), \quad n = 1, 2, \dots, \quad (5)$$

$$2n - 1 \ll \ln(\frac{8}{\Phi}).$$

The values of $\omega_s^{(n)}$ obtained from simulations at $\Phi = 0.2$ (see Fig. 3) are in a good agreement with the formula (4). As concerns the values of $h_{gc}(\omega_s^{(n)})$, the value $\Phi = 0.2$ is too large for Eq. (5) to be valid but, even so, Eq. (5) provides the correct order of magnitude for $h_{gc}(\omega_s^{(1)})$ and $h_{gc}(\omega_s^{(2)})$ (see Fig. 3). More accurate numerical calculations within the resonance approximation (cf. [5,6]) yield the value $h_{gc}(\omega_s^{(1)}) \approx 0.005$, which practically coincides with the value measured in simulations.

It is worth mentioning two immediate generalizations:

1. The absence of pronounced spikes at the *even* harmonics (i.e. at $2n\omega_m$) is explained by the fact that the even Fourier harmonics of coordinate are equal to zero due to the symmetry of the potential (1) and therefore [1–6] there are no resonances of even order; for a non-symmetric potential, even-order resonances do exist so that spikes in $h_{gc}(\omega_f)$ at $\omega_f \approx 2n\omega_m$ exist also.

2. If the time-periodic driving is multiplicative rather than additive, then the resonances become *parametric*

(cf. [18]). Parametric resonance is more complicated and much less studied than nonlinear resonance. But, still, the major mechanism for the onset of global chaos remains the same, namely the combination of the reconnection between resonances of the same order and of their overlap in energy with the chaotic layers associated with the barriers. At the same time, the frequencies of the major spikes in $h_{gc}(\omega_f)$ are twice as large as those of the corresponding spikes in the case of the additive driving: this is because the characteristic frequencies of parametric resonance are typically doubled as compared with the nonlinear resonance (cf. [18]). Thus, if the parameter Φ in $U(q)$ (1) is periodically driven (which may correspond e.g. to the time-periodic electric force being perpendicular to the direction of the periodicity of the magnetic field [10,11]) i.e. if the full Hamiltonian is

$$\begin{aligned} H &= p^2/2 + (\Phi - \sin(q))^2/2, \\ \Phi &= \Phi_0 + h \cos(\omega_f t), \quad \Phi_0 = \text{const}, \end{aligned} \quad (6)$$

then one may expect for major spikes in $h_{gc}(\omega_f)$ to be at

$$\omega_{sp}^{(n)} \approx 2\omega_s^{(n)} \approx 2(2n-1)\omega_m, \quad n = 1, 2, \dots, \quad (7)$$

which agrees well with results of simulations.

Finally, we suggest two examples of physical applications: (i) a jump-wise increase of the *dc conductivity* occurs due to the jump-wise increase of the range of energies involved in the unbounded chaotic transport of electric charge carriers in a magnetic superlattice (cf. [10]); (ii) a significant decrease of the *activation energy* for noise-induced multi-barrier escape in the presence of periodic driving is associated with the noise-free transport from the lower barrier to beyond the upper barrier (cf. [19,6]).

In conclusion, we have generalized the Chirikov resonance-overlap criterion for zero-dispersion systems, in particular for systems with more than one separatrix, and we have shown that the onset of global chaos may occur at extremely small magnitude of perturbation, unlike the conventional case.

The work was supported by INTAS Grants 97-574 and 00-00867. We are grateful to P.V.E. McClintock and K. Richter for discussions.

- [6] S.M. Soskin, R. Mannella, P.V.E. McClintock, "Zero-dispersion phenomena", submitted to "Phys. Rep."
- [7] J.E. Howard and S.M. Hohns, Phys. Rev. **A** **29**, 418 (1984).
- [8] J.E. Howard and J. Humpherys, Physica **D** **80**, 256 (1995).
- [9] D. del-Castillo-Negrete, J.M. Greene, P.J. Morrison, Physica **D** **61**, 1 (1996).
- [10] O.M. Yevtushenko and K.Richter, Phys. Rev. **B** **57**, 14839 (1998).
- [11] O.M. Yevtushenko and K.Richter, Physica **E** **4**, 256 (1999).
- [12] H.A. Carmona et al., Phys. Rev. Lett. **74**, 3009 (1995).
- [13] P.D. Ye et al., Phys. Rev. Lett. **74**, 3013 (1995).
- [14] G.J.O. Schmidt, Phys. Rev. **B** **47**, 13007 (1993).
- [15] P. Shmelcher, D.L. Shepelyansky, Phys. Rev. **B** **49**, 7418 (1994).
- [16] The major qualitative conclusions of our paper are not sensitive to a type of a perturbation, in particular of its dependence on q . To be concrete, we put the latter to be $\propto q$ in (2): for the 2D electron gas, it is relevant if a time-periodic electric force is applied parallel to the direction of periodicity of the magnetic field [11].
- [17] In the figure, we still use two colours for the different parts of this trajectory in order to demonstrate that their mixing occurs very slowly, which indicates that the given h is just slightly above the critical value h_{gc} .
- [18] L.D. Landau and E.M. Lifshitz, Mechanics (Pergamon, London, 1976).
- [19] S.M. Soskin, R. Mannella, A.N. Silchenko, unpublished.

- [1] B.V. Chirikov, Phys. Rep. **52**, 263 (1979).
- [2] A.J. Lichtenberg, M.A. Liebermann, Regular and Stochastic Motion (Springer, New York, 1992).
- [3] G.M. Zaslavsky, R.D. Sagdeev, D.A. Usikov and A.A. Chernikov, Weak Chaos and Quasi-Regular Patterns (Cambridge University Press, 1991).
- [4] S.M. Soskin, Phys. Rev. E **50**, R44 (1994).
- [5] S.M. Soskin et al., International Journal of Bifurcation and Chaos **7**, 923 (1997); R. Mannella, S.M. Soskin and P.V.E. McClintock, *ibid.* **8**, 701 (1998).

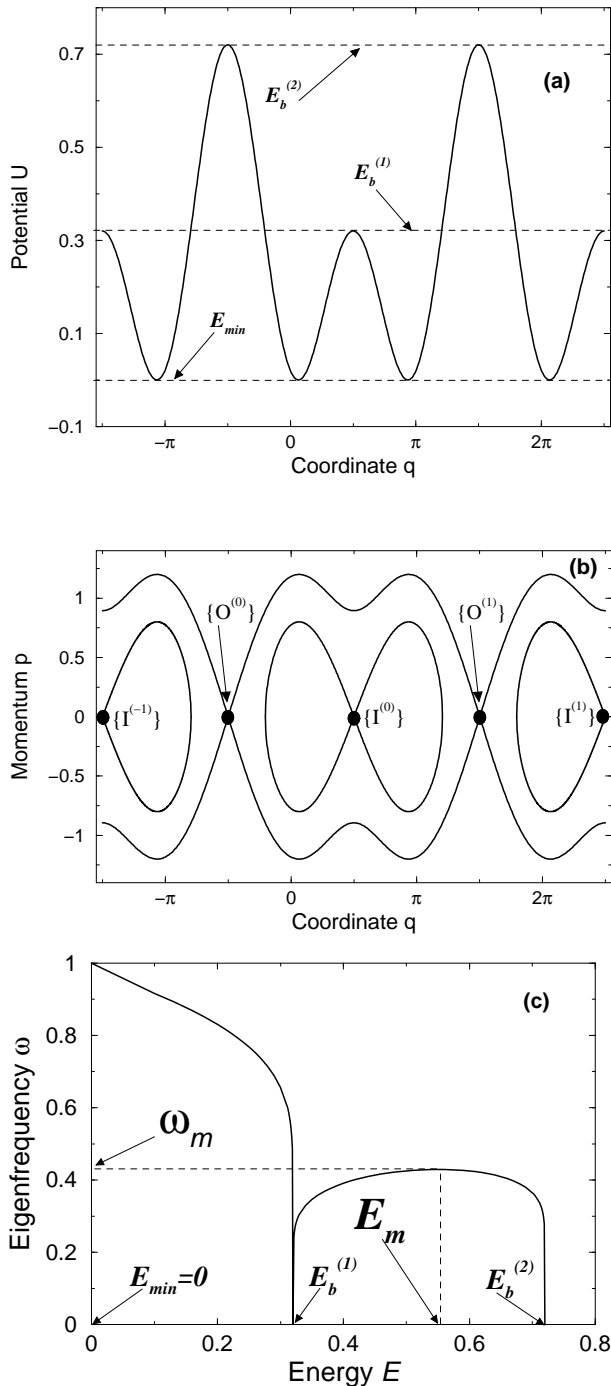


FIG. 1. The potential $U(q)$, the separatrices in the phase space and the eigenfrequency $\omega(E)$ for the unperturbed Hamiltonian system (1) with $\Phi = 0.2$, in (a), (b) and (c) respectively. In (a), $U(q)$ is shown by the solid line while the barriers levels and the minimal energy are shown by the dashed lines and indicated additionally by the labels $E_b^{(1)}$, $E_b^{(2)}$ and E_{min} respectively. In (b), the separatrices (corresponding to the barriers levels) are shown by the solid lines while the saddles are additionally indicated by dots and labels $\{I^{(l)}\}$ and $\{O^{(l)}\}$, for the inner and outer separatrices respectively (the superscript is introduced to resolve different 2π -periods in q). In (c), $\omega(E)$ is shown by the solid line while the extreme eigenfrequency ω_m and the corresponding energy E_m are indicated by the dashed lines and by the labels.

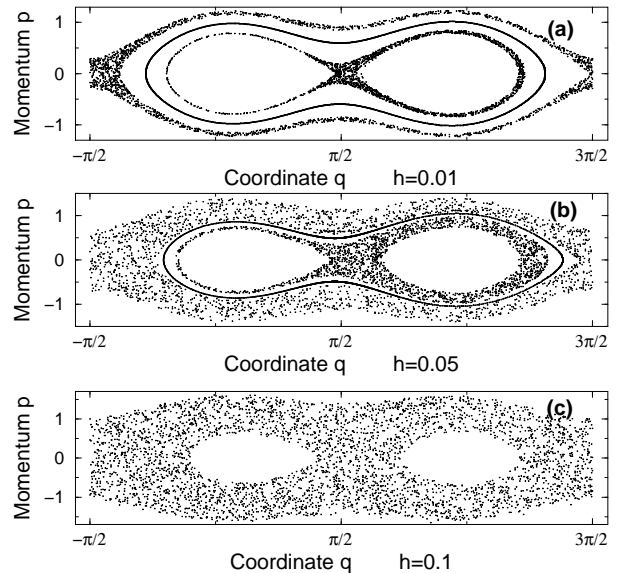


FIG. 2. The evolution of the stroboscopic (for instants $n2\pi/\omega_f$ with $n = 0, 1, 2, \dots$) Poincaré sections of the system (2)-(1) at $\Phi = 0.2$, with $\omega_f = 0.3$ while h grows from the top to the bottom: (a) 0.01, (b) 0.05, (c) 0.1. The number of points in each trajectory is 2000 (i.e. the integration time is $4000\pi/\omega_f$). In parts (a) and (b), three characteristic trajectories are shown: the inner trajectory starts from the state $\{I^{(0)}\} \equiv \{p = 0, q = \pi/2\}$ (which corresponds to the inner saddle of the unperturbed system), and is chaotic but bounded in the space; the outer trajectory starts from $\{O^{(0)}\} \equiv \{p = 0, q = -\pi/2\}$ (which corresponds to the outer saddle of the unperturbed system), and is chaotic and unbounded in coordinate; the third trajectory represents an example of a regular (KAM) trajectory separating the above chaotic ones. In (c), only one, chaotic and unbounded, trajectory exists in the relevant region of the Poincaré section.

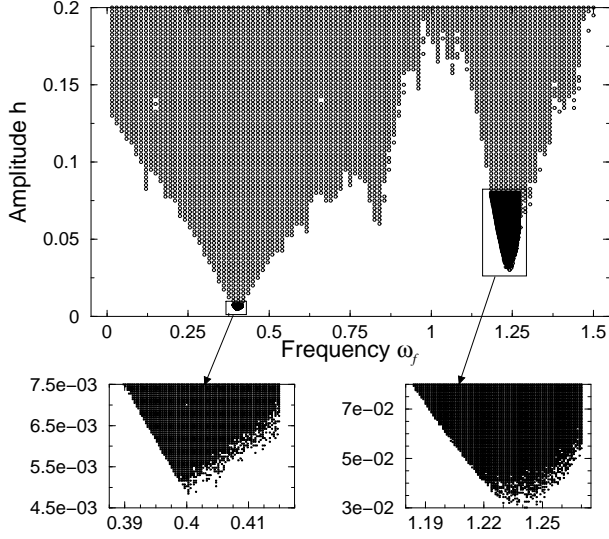


FIG. 3. The bifurcation diagram indicating (by shading) the parameter ranges for which there is global chaos: the latter is tested in simulations by noting whether the system can be transported from the state $\{I^{(0)}\} \equiv \{p = 0, q = \pi/2\}$ (the inner saddle) beyond the neighbouring outer saddles, $\{O^{(0)}\}$ and $\{O^{(1)}\}$, i.e. if the coordinate reaches either $-\pi/2$ or $3\pi/2$. The grid in the regions bounded by the rectangles was made significantly denser than beyond them in order to find more accurately the boundaries of the “chaotic” spikes. The integration time for each point of the grid is 12000π .

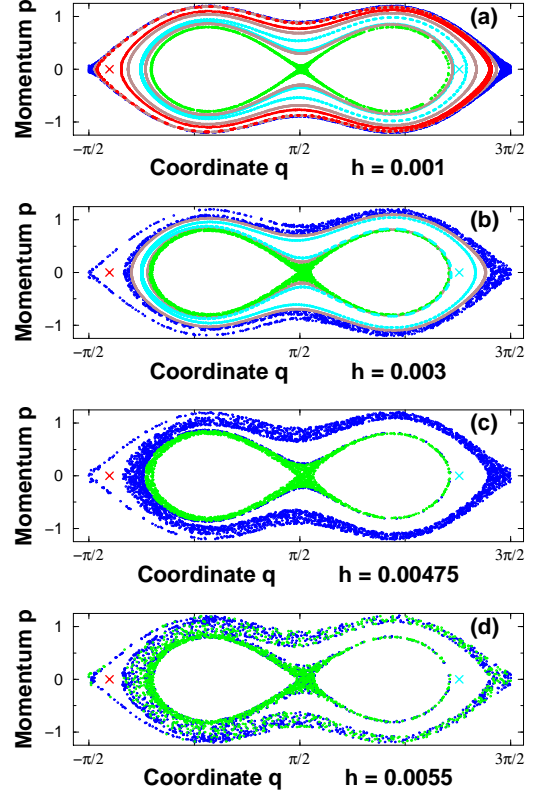


FIG. 4. The evolution of the stroboscopic (for instants $n2\pi/\omega_f$ with $n = 0, 1, 2, \dots$) Poincaré section of the system (2)-(1) with $\Phi = 0.2$ as the amplitude of the perturbation h grows while the frequency is fixed at $\omega_f = 0.401$. The number of points in each trajectory is 2000. The chaotic trajectories starting from the states $\{I^{(0)}\}$ and $\{O^{(0)}\}$ are drawn in green and blue respectively. The stable stationary points (the 1st-order nonlinear resonances) are indicated by the red and cyan crosses. The chaotic trajectories associated with the resonances, in those cases when they do not merge with the green/blue chaotic trajectories, are indicated in red and cyan respectively (their real width is exponentially small and much less than the width of the line as drawn). Examples of KAM trajectories embracing the state $\{I^{(0)}\}$ while separating various chaotic trajectories are shown in brown.